



Updated dendrochronology and axial variation of climatic sensitivity in *Sequoiadendron giganteum*

Allyson L. Carroll¹ · Stephen C. Sillett¹

Received: 21 June 2023 / Accepted: 30 March 2024
© The Author(s) 2024

Abstract

Key message Dendroclimatic sensitivity varies by axial position for *Sequoiadendron giganteum*: negative correlations with June temperature strengthen with height, while positive correlations with snow water are strongest in the lower trunk.

Increment cores collected along trunks of mature *Sequoiadendron giganteum* provide new and updated ring-width chronologies ideal for assessing how height above ground affects sensitivity of radial growth to climatic variation. Chronologies from 61 living trees at nine locations across the geographic distribution span 1973 yr. Analyses of subsets of 18–44 trees reveal that correlations between radial increments and climate (temperature, water availability) vary with axial position. Negative correlations with maximum and minimum June temperature intensify with height and are strongest at the highest position analyzed (60 m above ground). Sensitivity to the hydroclimate variable of April–1 snow water equivalent is stronger at lower trunk positions (10 m) compared to breast height or the upper trunk, and a similar relationship is identified for the standardized precipitation evapotranspiration index using a 12-month window ending in September. Drought-induced low-growth years computed as radial increment relative to the mean of 10 yr before and after are more weakly expressed at breast height compared to higher on the trunk (10–60 m). Analysis of regional upper (maximum core height = 87 m) versus lower trunk (above buttress) chronologies corroborate differing inter-annual correlations with climate depending on height above ground. Accounting for axial variation in dendroclimatic sensitivity can maximize the quality of environmental reconstructions using tree rings and improve biophysical understanding of *Sequoiadendron*, especially in the context of an increasingly arid climate.

Keywords *Sequoiadendron giganteum* · Dendrochronology · Climatic sensitivity · Height gradient

Introduction

Relationships between tree rings and climate underpin environmental reconstructions (e.g., Cook et al. 2007) and eco-physical understanding of species' stressors (e.g., Gazol et al. 2020), which are increasingly important in a warming climate (Pierce et al. 2018). Such foundational linkages are commonly based on samples from lower positions on trunks, most often at breast height (BH, 1.4 m), where long series from living trees are easily accessible from the ground. A

growing body of evidence based both on stem analysis of dead trees (e.g., Zhang et al. 2020) and rope-based sampling of living trees (e.g., Ishii et al. 2017) points to the limitations of lower trunk samples for quantifying growth of whole trees. Biomass increments estimated by diameter changes at BH compared to measurements across the height gradient are generally biased for tall species (Sillett et al. 2015a, b, 2019a, 2020), suggesting that whole-trunk sampling may be necessary to characterize climate–growth relationships.

Tree-ring formation occurs as carbon is invested in various components (e.g., trunks, branches, roots) via xylogenesis, a dynamic process that involves both internal (e.g., hormones) and external (e.g., climate) controls during various phases of cell formation in the vascular cambium (De Micco et al. 2019). Climate influences growth via availability of resources (e.g., water) and rates and timing of physiological processes (e.g., temperature-influenced cambial reactivation,

Communicated by S. Leavitt.

✉ Allyson L. Carroll
allyson.carroll@gmail.com

¹ Department of Forestry, Fire, and Rangeland Management, Cal Poly Humboldt, Arcata, CA 95521, USA

hormone concentrations; Fritts 1976; Vaganov et al. 2011; Begum et al. 2013; St. George 2014; Rathgeber et al. 2016). Climatic constraints on wood formation may differ along the main trunk due to factors such as phloem transport of sugars and hormones across long distances and increasing water stress with height above ground (Speer 2010; Kerhoulas and Kane 2012; Buttò et al. 2020). As trees grow taller, water entering via roots must be transported farther upward through the xylem to sustain photosynthesis and transpiration as gravity and friction resist its movement, diminishing stem turgor (Koch et al. 2004; Woodruff et al. 2004). In response to excessive water stress, trees close leaf stomata to stop transpiration (which curtails photosynthesis) and sustain stem turgor (McDowell et al. 2008; Peters et al. 2023). Radial growth is controlled by source limitations (i.e., availability of photosynthate) and by a tree's inability to convert photosynthate to biomass when stem turgor is too low for cell division and enlargement in the vascular cambium (sink limitations; Körner 2015; Rathgeber et al. 2016). Both source and sink limitations are influenced by climate (Zweifel et al. 2021; Cabon et al. 2022).

Dendroclimatic sensitivity varies by trunk axial position, and, while the direction of relationships is generally consistent among heights, the nature of this variation is not uniform among species. For *Pinus ponderosa*, the relative strength of models explaining climatic parameters (temperature, drought, water year precipitation) based on radial increments declines with height from treetops (22 m) followed by base of live crown (10 m) then BH (Kerhoulas and Kane 2012). Stem analysis of 389 *Pinus contorta* shows that upper trunk radial increment is related to conditions during the year of growth (e.g., early summer temperature, late winter to early spring moisture), while lower trunk radial increment is related to conditions in prior seasons (Chhin et al. 2010). For *Picea schrenkiana*, relationships between radial increment and temperature are weaker at BH than upper positions to 20 m (Zhang et al. 2020). Assessment of *Abies alba* and *Picea abies* at three positions up to 16.7 m reveals that BH series are not comparably sensitive to climate, with species- and altitude-specific differences (van der Maaten-Theunissen and Bouriaud 2012). In addition to varying axial relationships for conifers, the angiosperm *Fagus sylvatica* shows climate-related differences in growth partitioning between the trunk and crown (Latte et al. 2016) and growth prioritization in the upper stem during drought conditions (Peters et al. 2020). Drought response of nine deciduous and coniferous species show inconsistencies along the main stem (up to 29 m) with less pronounced responses with increasing stem height for most species (Hoffmann et al. 2018).

Sequoiadendron giganteum (giant sequoia) is well-suited for investigation of dendroclimatic variation along the trunk given its extreme height (up to 96.5 m, Sillett et al. 2021), strong crossdating, and extensive dendrochronological

history. *Sequoiadendron* is a foundational species of modern dendrochronology (Douglas 1919) known for generally com-
 placent annual rings punctuated by strong, narrow marker years that support multi-millennial ring-width chronologies with regional coherence of signal (Brown et al. 1992). While radial increments show positive but not robust inter-annual correlations with growing season drought metrics (Carroll et al. 2014), prominent low-growth years correspond with extremely arid conditions and have been used to assess regional drought frequency over millennia (Hughes and Brown 1992). Inter-annual sensitivities also reveal consistent negative relationships between ring indices and maximum and minimum temperature in June (Carroll et al. 2014). These relationships make sense in the context of a species growing in wet geomorphic locations amid an overarching climate of cool, wet winters followed by warm, dry summers in California's Sierra Nevada (Ray 2016). *Sequoiadendron* tree rings have been used to reconstruct snow water equivalent (SWE) as melting snow provides water during dry summer months (Touchan et al. 2021); while precipitation as snow, which may not fully reflect snowpack, lacked significant relationships (Wang et al. 2012; Carroll et al. 2014) and only 2–4% of precipitation falls after snowmelt (Sillett et al. 2019b).

As *Sequoiadendron* grows in drought-prone environments, it has several adaptations to alleviate water stress exacerbated by great height. Phenotypic plasticity of *Sequoiadendron* foliage exhibits environmental responsiveness whereby denser upper crown foliage is better able to withstand water stress via succulence, low surface area-to-volume ratios, and specialized leaf anatomy (Chin and Sillett 2016). A suite of leaf- and crown-level physiological mechanisms, including strong stomatal regulation, seasonal redistribution of leaf water, leaf toughening, and leaf shedding help *Sequoiadendron* maintain favorable water status during drought (Ambrose et al. 2015, 2018). These strategies likely contributed to the relatively low mortality rate of *Sequoiadendron* (albeit with unprecedented levels of foliage dieback; Stephenson et al. 2018) compared to other mixed conifers of the Sierra Nevada during the 2012–2016 hotter drought (Nydick et al. 2018). Although morphological, anatomical, and physiological adjustments allow *Sequoiadendron* to regulate water status (Ambrose et al. 2016), hydraulic limitations associated with great height may control carbon allocation and radial increments along the trunk.

The preponderance of dendrochronological study of *Sequoiadendron* has utilized ground-based sampling of increment cores from live trees or sections from dead trees. Targeting positions close to ground level increased the likelihood of accessing preserved fire scars and facilitated creation of a 3000-yr fire history (Swetnam et al. 2009). Fire-affected sections often show growth irregularities, and these were generally avoided for the SWE reconstruction

(Touchan et al. 2021). Nevertheless, samples acquired near bases of large trees, even away from fire scars, can influence the expression of growth rings by virtue of irregular morphology. For example, *Sequoia sempervirens* (Carroll and Sillett 2023) and four eucalypt species (Brookhouse and Brack 2008) show reduced inter-series correlation at basal compared to upper trunk positions. As the largest tree species on Earth, lower trunks of *Sequoiadendron* can have highly irregular shapes with pronounced buttressing and fire caves (Sillett et al. 2019b) that may hinder expression of climate-induced ring-width variation.

Recent work on *Sequoiadendron* utilizing rope-based techniques for whole-trunk sampling permits spatially explicit assessment of this species. Initial sampling at six locations supported baseline ring-width chronologies, climatic sensitivity analysis, as well as quantification of tree age, biomass, and development (Carroll et al. 2014; Sillett et al. 2015b). Additional cores from the same trees (for biomass increment; Sillett et al. 2019b) as well as new trees (Sillett et al. 2021; Williams et al. 2021) increase replication and promote extension of millennial-length *Sequoiadendron* chronologies. Such chronologies fit within a rich chronicle for this species and can be assessed for their signal strength and regional coherence. Selection of trees with suitable within-trunk replication allows for appraisal of dendroclimatic relationships across the axial (trunk height) gradient. Given *Sequoiadendron*'s propensity for intermittent but prominent low-growth years, axial variation in the expression of such years is relevant to consider. Here we update and expand *Sequoiadendron* chronologies and investigate how dendroclimatic sensitivity and relative increments during low-growth years vary by height above the ground.

Methods

Tree selection and sampling

A total of 61 living *Sequoiadendron* from nine forest locations were studied from 2005–2020 for various research objectives (Carroll et al. 2014; Sillett et al. 2015b, 2019b, 2021; Williams et al. 2021; Tables 1 and S1). Locations spanned the 150 km² geographic distribution of *Sequoiadendron* groves (Table 1), including the South Grove of Calaveras Big Trees State Park (CBT), Mariposa Grove in Yosemite National Park (MAR), Redwood Mountain Grove in Kings Canyon National Park (RMG), the adjacent Whitaker Forest managed by the University of California (WF), Giant Forest in Sequoia National Park (GF), Mountain Home Grove in Mountain Home Demonstration State Forest (MH), and Freeman Creek, Red Hill, and Alder Creek Groves in Giant Sequoia National Monument (FC, RH, AC). *Sequoiadendron* generally occupies wet topographic positions, including adjacent to perennial streams and meadows pooling water from granitic plateaus, though some trees were growing upland farther from surface water. All study locations (except AC) are further described elsewhere (see Sillett et al. 2015b, 2019b).

Trees ranged from 26.1–96.5 tall (mean = 74.2 m), 39–814 cm *f*DBH (functional diameter at breast height, or diameter of a circle with equivalent area, mean = 409 cm), and 100–3298 yr old (mean 1077 yr, see Sillett et al. 2019b for description of age calculations beyond innermost cross-dated rings), and most trees occupied dominant or co-dominant crown positions (Table S1). Increment cores were collected at regular intervals along main trunks, and positions above breast height (BH, 1.4 m) were accessed via free-hanging ropes. Generally, each height had 2 cores or 3–4 cores when trunk diameters exceeded 2 or 3 m, respectively. Irregularities (e.g., branch collars, fire occlusions)

Table 1 Description of nine *Sequoiadendron* study locations sequenced from north to south

Location	Lat. (°N)	Long. (°W)	Elev. (m)	Jun Tmin–Tmax (°C)	Precip (cm yr ⁻¹)
CBT	38.25	120.24	1480–1530	8.6–23.8	126
MAR	37.51	119.60	1750–2000	6.2–21.0	106
WF	36.70	118.93	1640–1820	5.9–20.9	104
RMG	36.69	118.91	1680–1700	5.9–20.9	104
GF	36.56	118.74	2090–2150	2.2–16.1	104
MH	36.21	118.67	1960–1970	9.2–22.0	90
AC	36.19	118.62	1900–2100	7.2–20.6	107
FC	36.14	118.52	1860–1890	4.9–20.9	108
RH	36.08	118.61	1960–2010	8.2–21.7	96

See text for location acronyms. Tmin and Tmax are average June minimum and maximum temperature, and precip is average annual precipitation (4-km PRISM data; 1900–2021)

were avoided as much as possible, and cores were generally evenly spaced around the circumference. Trees at AC and RH had shallow cores at BH and top of buttress (TB), and deeper cores aiming for pith at 10-m increments from 10 m to treetop. Trees at MAR followed the same regimen but had no cores below 10 m. Five locations (CBT, RMG, GF, MH, FC) with 1-ha plots trees were regularly sampled from BH to treetop with some variation in collection height, and 21 of these trees were re-sampled at ~5-yr intervals near the original coring positions (Sillett et al. 2019b), providing series to update previously published chronologies (Carroll et al. 2014). Within-tree sampling at WF was most variable due to disparate research goals. Core sampling followed the dominant reiterated (i.e., resprouted) trunk toward treetop when applicable.

Crossdating and chronologies

Cores were dried, glued to wooden mounts, sanded with progressively finer grit (> 600), and inspected under a stereo microscope to discern ring boundaries. Ring widths were measured to 0.001 mm using WinDendro software (v.2009b, Régent Instruments Inc., Québec, Canada) with images at 1200 dpi from an EPSON Expression 10000XL scanner. Crossdating occurred by listing visual marker years with statistical validation via staggered correlation analysis using Cofecha software (Holmes 1983) and proceeded, first, among cores within a tree, then, between trees per location. Crossdating was categorized for all years following previously defined protocol (Carroll et al. 2014; Carroll and Sillett 2023) and differentiated between series with high and moderate confidence to identify sections with some ambiguity (e.g., Lorimer et al. 1999).

Due to intensive within-tree sampling, chronologies were generated for each of 61 trees and then combined accordingly for nine locations and one regional chronology. Tree chronologies included series with high confidence in crossdating and ≥ 30 yr length. Series were standardized to ring-width indices via ARSTAN (Cook 1985) using a cubic smoothing spline with a 50% frequency cutoff at 32 yr (32-yr spline) to remove geometric growth trends and low-frequency variation. Standard (STD) tree chronologies were combined into nine respective location chronologies and one composite chronology with no further detrending and used a biweight robust mean to reduce the influence of outliers (Cook and Kairiukstis 1990). Chronology statistics of r_{bar} (mean between-tree or between-series correlation, as applicable) and expressed population signal (EPS) were calculated with dplR library in R (Bunn 2008; R Core Team 2023). EPS expresses signal strength, depends on sample depth and r_{bar} , and has a commonly used threshold of 0.85 (Wigley et al. 1984). We used Sierra Nevada regional ring-width data spanning 23 locations from the International

Tree-Ring Data Bank (CA726; Touchan et al. 2021) as a comparison for inter-annual variation to confirm crossdating. The 260 raw series from CA726 were detrended in the same manner described above to generate an analogous chronology. Staggered Pearson correlation analysis on overlapping 50-yr segments via Cofecha produced comparative statistics among chronologies.

Dendroclimatic relationships

Key climatic variables were selected based on previous study (Hughes and Brown 1992; Carroll et al. 2014; Touchan et al. 2021) and included June minimum temperature (Tmin), June maximum temperature (Tmax), a drought index, and snow water equivalent (SWE, amount of water in snowpack). We confirmed inter-annual relationships between location chronologies (STD) and climate using bootstrapped Pearson's correlation analysis with the treeclim package in R (Zang and Biondi 2015).

For location-specific June Tmin and Tmax, we used 4-km monthly PRISM data (1900–present; PRISM Climate Group 2023, www.prism.oregonstate.edu, accessed 1 May 2023). All temperature records were detrended with a 32-yr spline to focus on inter-annual variation. For the location-specific drought index, we utilized standardized precipitation evapotranspiration index (SPEI) using a 12-month window ending in September. SPEI z-values (1902–2018) were acquired from the CSIC database via KNMI Climate Explorer (<http://climexp.knmi.nl>, accessed 3 May 2023) for each location with 0.5-degree spatial resolution. SPEI is a multi-scalar index that considers precipitation and potential evaporation, incorporating a temperature component (Vicente-Serrano et al. 2010). Values for April-1 SWE volume for the southern Sierra Nevada (1940–2018) were based on multiple data streams of snow reanalysis and in situ snow courses via Huning and AghaKouchak (2020). Regional temperature and SPEI data were generated using KNMI Climate Explorer for CSIC and PRISM data, respectively.

Height-related climatic sensitivity and expression of low-growth years

We conducted a tree-level analysis of climatic sensitivity and expression of low-growth rings with a complete block design using radial increments at regular height intervals along the main trunk. Two complementary datasets were utilized: trees with representative rings at (1) BH, 10 m, and 10-m intervals to 60 m above ground and (2) 10–60 m above ground at 10-m intervals. Inclusion of shallow BH cores limited the number of trees with a complete dataset to analyze but incorporated this important position. Trees were considered for analysis if they had cores at each height or interpolated rings based on cores ≤ 10 m both above and

below sampling height. For the 33 trees used in axial analyses, mean distance from target height was 0.2 m, and 13 trees had interpolated rings for 1, 2, or 3 heights. All positions were on main trunks except one 60-m position on a reiterated trunk with a cambial age of 982 yr. These 33 trees represented nine locations, ranged from 65.5–96.5 m tall (mean = 78.7 m), 229–814 cm *f*DBH (mean = 470 cm), and 305–2531 yr old (mean = 1353 yr; Table S1).

To generate radial increments, ring widths from replicate cores per height were averaged and extended as far back in time as possible using local relationships between multi-core averages when only single cores remained. Wood radius at measurement height was computed by subtracting adjusted bark radius from total radius, where bark radius was first predicted from diameter and height using equations for *Sequoiadendron* (Sillett et al. 2015b) and then adjusted by scaling relationships between observed and predicted radii. Measured rings were scaled to fresh widths using the ratio of freshly extracted and mounted core lengths (± 1 mm) per location. The sum of measured ring widths from cambium to pith (if reached) was forced to equal wood radius. Wood radii were decremented by annual rings across the trunk height gradient with rings at intervening heights of measurement (no crossdated core samples) computed by interpolation. Rings with high and moderate confidence in crossdating were utilized almost exclusively. In the few instances when crossdating was not achieved, increments were interpolated from the nearest dated series.

We calculated Pearson's correlation coefficients between location-specific climatic variables and ring indices at each axial position for trees with suitable data. To control for long-term growth trends and varying cambial ages along the trunk, we detrended and standardized radial increments per height with a 32-yr spline via *dplR* (Bunn 2008). Years considered vary depending on climate records and last year of ring indices with maximum windows of 1940–2018 for SWE and 1900–2019 for Tmax, Tmin, and SPEI. To determine if correlations differed among heights, we used non-parametric Friedman's rank sum tests in an unreplicated, complete block design (tree as blocking variable, height as group, correlation coefficient as dependent variable). Differences between categories were evaluated with exact post hoc tests for all pairwise comparisons of Friedman rank sums (Eisinga et al. 2017) with *P* value adjustment for multiple comparisons to control for false discovery rate (Benjamini and Hochberg 1995). Tests were run using *stats* and *PMCRplus* packages in R (Pohlert 2022; R Core Team 2023).

We determined if expression of low-growth years differed among heights using proportional radial increment (PRI) as the dependent variable in the Friedman's rank sum test, run with the same method described in the preceding paragraph. For each low-growth year per height, PRI was calculated as the radial increment of the low-growth year divided by the mean

radial increment for the 10 years before and after to provide a relativized metric. Low-growth years were defined as those with the smallest radial increments per tree selected from the common period shared by all axial positions under investigation (BH to 60 m; 10–60 m). Up to 3 low-growth years were analyzed per tree if the ring index exceeded two standard deviations below the mean for the common period based on the STD tree chronology. For years near the end of series (e.g., 2014), as many years as remained were used. If multiple low-growth years were identified in the 10-year window (e.g., 2014 and 2015), then only the narrowest was considered per tree. To eliminate pseudo-replication, PRI was averaged at each height per tree ($N = 33$).

In addition to the tree-specific analysis, we compared composite chronologies per height interval with regional climatic variables. The robust biweight mean was used to combine detrended radial increments into the STD version of height-specific chronologies via *dplR* (Bunn 2008). Height-specific chronologies were generated using the same trees as the BH to 60 m ($N = 18$) and 10–60 m ($N = 31$) analyses. We used bootstrapped Pearson correlation analysis via *treeclim* in R to assess relationships between height chronologies and regional climatic variables (1940–2011 for SWE; 1902–2011 for Tmax, Tmin, and SPEI).

Climatic sensitivity of upper vs. lower trunk

To increase tree replication, we relaxed delineation of axial positions from 10-m intervals to two categories (upper vs. lower trunk) and used 44 trees with representative cores at both positions spanning 1900–2011 (Table S1). Upper trunk was the highest position on the trunk below any reiterations (mean = 63 m, range 40–87 m). Lower trunk was the lowest position at or above the top of buttress (mean = 13 m, range 8–31 m). Only measured ring widths crossdated with high confidence were used (no interpolations). A target of two cores were selected per position, but five trees had only one core per position. If more than two cores were eligible, we chose those with strong crossdating correlations (via *Cofecha* outputs) and similar radial position (e.g., azimuth) between upper and lower trunk cores. We combined series into STD versions of upper and lower trunk regional chronologies, detrended with a 32-yr spline to focus on inter-annual variation as previously described, and, again, used bootstrapped correlation analysis in *treeclim* to generate Pearson coefficients with regional climatic variables.

Results

Ring-width chronologies

Standardized ring indices for 61 *Sequoiadendron* (mean = 19 series) supported three new (MAR, AC, RH) and six updated (CBT, WF, RMG, GF, MH, FC; Carroll et al. 2014) location chronologies ranging 928–1973 yr in length (Table 2, S1, S2). Tree-level crossdating was near complete (98.6 ± 0.3 and $0.5 \pm 0.2\%$ rings dated with high and moderate confidence, respectively; mean ± 1 SE) with $0.15 \pm 0.04\%$ missing rings. Chronology lengths exceeded 1000 yr for 17 trees and 500 yr for 36 trees (Table S1). Location chronologies were composed of 4–18 trees (mean = 134 series) and had robust signal strength ($r_{\text{bar}} = 0.521 \pm 0.02$, $\text{EPS} = 0.86 \pm 0.01$; Table 2). The oldest chronology (AC) reached the year 47 CE, but two-tree replication extended to 622 CE. The nine location chronologies expressed shared inter-annual variation with each other and with a pre-established composite chronology (CA276; Touchan et al. 2021): mean correlation for overlapping 50-yr segments ($N = 79$) exceeded 0.45 ($P \leq 0.001$) for 71 segments, and the lowest correlation ($r = 0.26$) was for the earliest century where AC had only one-tree replication (Fig. 1). Among chronologies, the innermost section of CBT was weakest with a mean correlation of 0.20 for overlapping segments from 719–825 CE. Strong crossdating and inter-location synchrony supported the development of a 61-tree regional chronology (47–2019 CE) with declining replication back in time but strong signal strength ($\text{EPS} \geq 0.85$) from 744 CE to present (Fig. 2). Sixty-five percent of years in the lowest decile of this robust portion were shared with the extreme drought years defined by Hughes and Brown's (1992) analysis of three locations. Raw measurements of ring widths for all series dated with high confidence (regardless of inter-series correlations) are provided in Table S3.

Confirmation of baseline climatic relationships

Inter-annual ring indices for *Sequoiadendron* at nine locations correlated with the four climate variables selected for investigation based on prior research (Fig. 3). Clear trends in direction of relationships were evident across locations: negative correlations with June Tmax and Tmin and positive correlations with SWE and SPEI. Correlation strength varied by location with most showing inter-annual relationships significant at $P < 0.05$ and some at $P < 0.001$. All locations expressed stronger relationships with June Tmax than Tmin, while SWE and SPEI were similar.

Table 2 Sampling intensities, crossdating summaries, and chronology statistics for nine *Sequoiadendron* study locations sequenced from north to south

Location	Samples (#)			Crossdating (%)			Chronology statistics						
	# trees	# series	# rings	High conf.	Mod conf	Not dated	Last year	First year	Length (yr)	Two-tree cutoff	MR (%)	rbar	EPS
CBT	7	140	58,727	96.3	1.9	1.9	2014	719	1296	784	0.08	0.475	0.864
MAR	6	66	48,274	98.5	0.2	1.2	2015	660	1356	904	0.07	0.507	0.860
WF	18	270	65,171	99.1	0.4	0.3	2012	1085	928	1204	0.15	0.412	0.926
RMG	4	96	40,256	97.1	0.6	2.3	2016	824	1193	926	0.10	0.499	0.799
GF	6	143	63,485	96.8	1.0	1.8	2015	474	1542	713	0.12	0.524	0.868
MH	5	108	43,988	99.0	0.2	0.8	2016	782	1235	831	0.03	0.626	0.893
AC	5	129	81,254	99.3	0.1	0.5	2019	47	1973	622	0.04	0.617	0.889
FC	5	153	43,045	98.4	0.3	1.3	2015	544	1472	1227	0.06	0.473	0.818
RH	5	104	53,905	98.0	0.0	1.6	2017	451	1567	1193	0.05	0.559	0.864

Tree-level chronologies used series ≥ 30 yr, high crossdating confidence, detrended with 32-yr spline. Standard versions combined into location chronologies. Two-tree cutoff is earliest year with two-tree replication. Missing rings (MR) for chronologies only include constituent series. Rbar (mean correlation between pairs of trees) and EPS (expressed population signal) are for the period common to trees per location

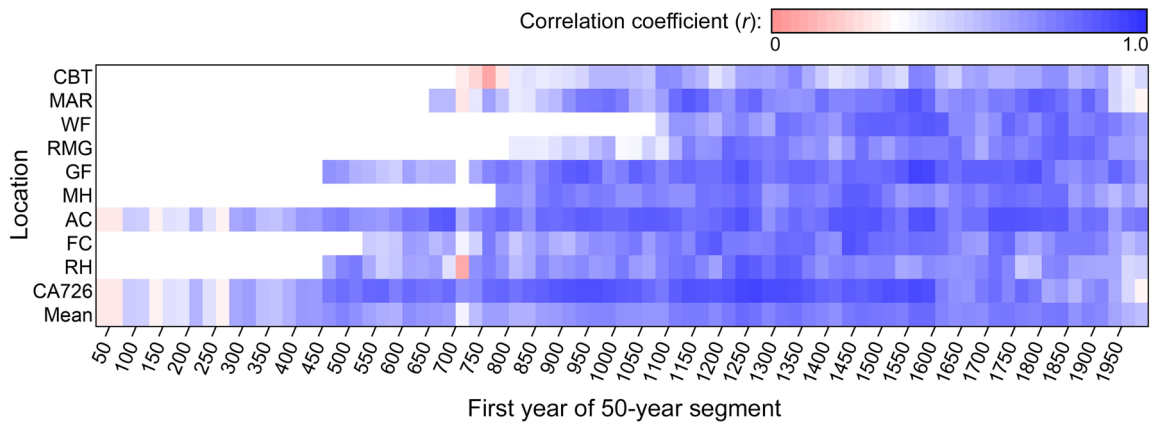


Fig. 1 Overlapping correlations among standardized ring-width indices for *Sequoiadendron* at nine locations and a composite chronology. Location IDs correspond to Table 1. The composite chronology was accessed via the International Tree-Ring Data Bank and is composed of 23 locations (CA726; Touchan et al. 2021). Pearson's correlation

coefficients (r) are for 50-yr segments lagged by 25 yr. Each cell represents a 50-yr segment, bottom number is first year of associated segment. Strength of colors corresponds to correlations, where white is $r=0.328$, the cutoff for one-tailed significance at $P=0.01$

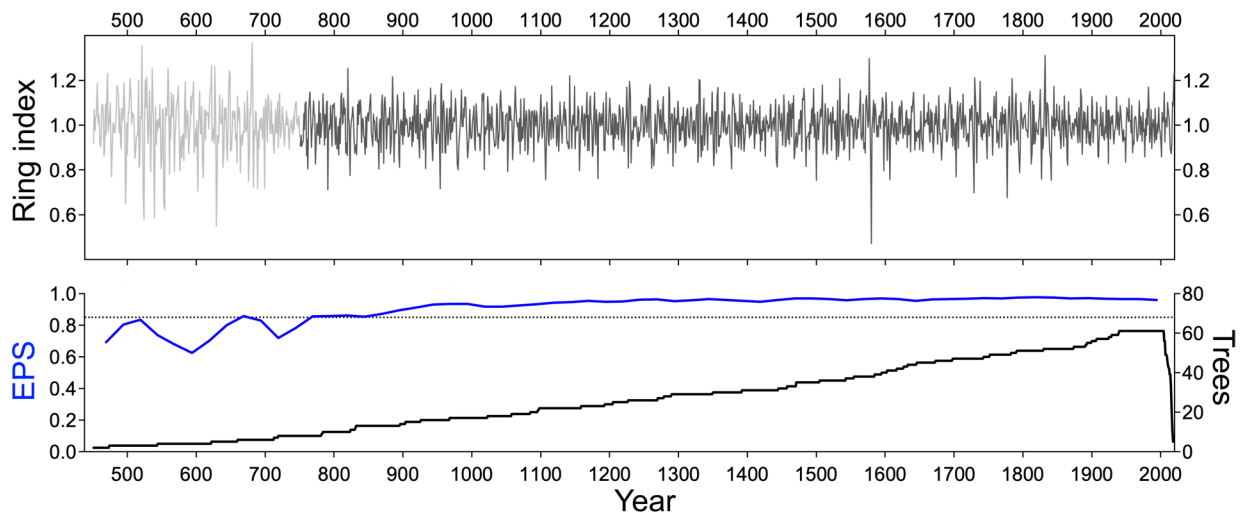


Fig. 2 *Sequoiadendron* chronology composed of 61 trees at nine locations across the species range with signal strength and sample depth. Tree-level chronologies are detrended with a 32-yr spline to focus on inter-annual variation, and standard versions are combined by robust biweight mean with no further detrending. Sample depth

conveys number of trees with ring indices and is truncated when < 2 trees. Expressed population signal (EPS), a metric of chronology representativeness, is shown in blue relative to a 0.85 threshold. Lighter gray ring indices correspond to EPS values < 0.85

Height-related climatic sensitivity and expression of low-growth years

Tree-level analysis showed that height above ground affected both climatic sensitivity and expression of low-growth years for *Sequoiadendron*. Specifically, differences were identified for correlations of radial increments with June Tmax, June Tmin, and SWE (but not SPEI), as well as for PRI of low-growth years compared to surrounding decades (Table 3), and pairwise comparisons indicated which categories differed using complementary analyses of 1.4–60 m

and 10–60 m. June Tmax exhibited the clearest trend of increasing sensitivity with height above ground ($N=31$; Fig. 4). Explained variance increased from BH (2.1%) to 60 m (7.5%, $N=18$). June Tmin exhibited similar but weaker trends: the 60-m position ranked higher than some lower positions (10, 20, 40 m; $N=31$) and BH ($N=18$). For correlations with SWE, BH ranked lower than 10 or 20 m positions ($N=18$). PRI for low-growth years was higher at BH (0.750) compared to all higher positions (0.647 ± 0.003 ; mean ± 1 SE) for the 18-tree analysis, while no differences were apparent among 10–60 m positions ($N=31$).

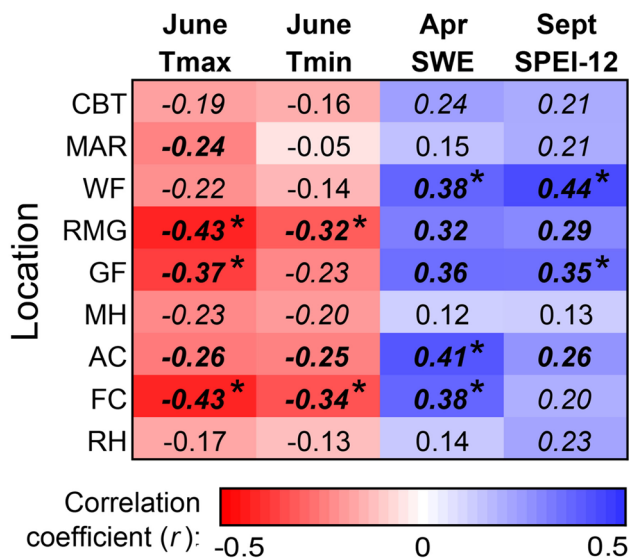


Fig. 3 Bootstrapped Pearson's correlation coefficients (r) between key climatic variables and inter-annual ring-width chronologies at nine locations for *Sequoiadendron*. Location IDs match Table 1. Climate variables are June maximum and minimum temperature (Tmax and Tmin, respectively), April 1 snow water equivalent (SWE), and standardized precipitation evapotranspiration index (SPEI) for the 12-month window ending in September. Window of analysis varies depending on climate record and last year of chronology (maximum window=1900–2019 for SPEI, Tmax, and Tmin; 1940–2018 for SWE). Levels of significance indicated by italics for $P < 0.05$, bold for $P < 0.01$, * for $P < 0.001$

Radial increments from the same trees ($N = 18$ and 31) were combined into height-specific chronologies for comparison with regional climatic variables, supplementing relationships expressed by tree-level analyses. June Tmax and

June Tmin showed generally increasingly negative correlations with height above ground with the strongest ($r = -0.44$, $P < 0.0001$) between June Tmax and the 60-m chronology composed of 31 trees (Table 4). Correlations were not significant ($P < 0.01$) for Tmax at BH or for Tmin at BH or 10 m for the 18-tree analysis. SWE correlated with lower trunk positions but not BH or heights ≥ 40 m ($P < 0.01$). The strongest relationship for SWE was with the 10-m chronology composed of 31 trees ($r = 0.45$, $P < 0.0001$). All positions showed positive relationships with SPEI ($P < 0.01$) with strongest correlations at 10 m for both analyses. Overall, we observed increasing variance explained by height for temperature variables and decreasing variance explained by height for hydroclimate variables, except for weak correlations at BH (Fig. 5). The maximum variance explained was at 60 m for June Tmax and Tmin and at 10 m for SWE and SPEI, but none exceeded exceed 20%.

Climatic sensitivity of upper vs. lower trunk

Upper and lower trunk chronologies representing 44 *Sequoiadendron* across the geographic distribution substantiated differing inter-annual sensitivities to climate depending on height above ground (Fig. 6). Relationships had similar directions, but the strength varied by trunk position. Upper trunk chronologies were negatively correlated with June Tmax and Tmin at $P < 0.001$, while lower trunk chronologies exhibited weaker correlations. Lower trunk chronologies (but above top of buttress) showed positive correlations with SWE at $P < 0.001$ while the upper trunk relationship was weaker ($P = 0.03$). Both upper and lower trunk chronologies

Table 3 Summary of Friedman's nonparametric rank sum tests for differences in climate sensitivities and expression of low-growth years by incremented axial positions in *Sequoiadendron*

Dependent variable	Trees (N)	Source of variation	df	χ^2	P
Tmax (June) correlation	18	Height (1.4–60 m)	6	21.91	0.001*
Tmax (June) correlation	31	Height (10–60 m)	5	30.02	<0.001*
Tmin (June) correlation	18	Height (1.4–60 m)	6	14.79	0.022
Tmin (June) correlation	31	Height (10–60 m)	5	19.13	0.002
SWE (Apr-1) correlation	22	Height (1.4–60 m)	6	17.49	0.008
SWE (Apr-1) correlation	32	Height (10–60 m)	5	11.75	0.038
SPEI-12 (Sept) correlation	18	Height (1.4–60 m)	6	8.83	0.183
SPEI-12 (Sept) correlation	31	Height (10–60 m)	5	6.80	0.236
PRI	24	Height (1.4–60 m)	6	17.88	0.007
PRI	33	Height (10–60 m)	5	9.64	0.086

Unreplicated, complete block design used with tree as blocking variable. Each dependent variable has two analyses: 1.4–60 and 10–60 m. Dependent variables are Pearson's correlation coefficients (r , between ring increment and climate metric) and proportional radial increment (PRI). $PRI =$ radial increment of low-growth year divided by mean increment of 10 yr before and after. Tmax (maximum temperature) and Tmin (minimum temperature) are for June, SWE (snow water equivalent) is for April 1, and SPEI (standardized precipitation evapotranspiration index) is for the 12-month window ending in September. $DF =$ degrees of freedom. $\chi^2 =$ Friedman Chi-squared test statistic. Levels of significance indicated by italics for $P < 0.05$, bold for $P < 0.01$, * for $P < 0.001$

Fig. 4 Sensitivity of radial growth to June temperatures varies by axial position (height above ground) for *Sequoiadendron* based on comparisons of Friedman rank sums. Values are squared Pearson's correlation coefficients (r , between ring increment and climate), expressing % variance. Window of analysis is 1900–2019 for June Tmax (maximum temperature) and Tmin (minimum temperature). Complementary analyses are presented for height categories from 10–60 m (left) and 1.4–60 m (right). Tree replication in Table 3. Bars show mean \pm 1 SE. Differences between heights determined by exact post hoc tests for all pairwise comparisons of Friedman rank sums. Categories not connected by same letter are significantly different ($P \leq 0.05$)

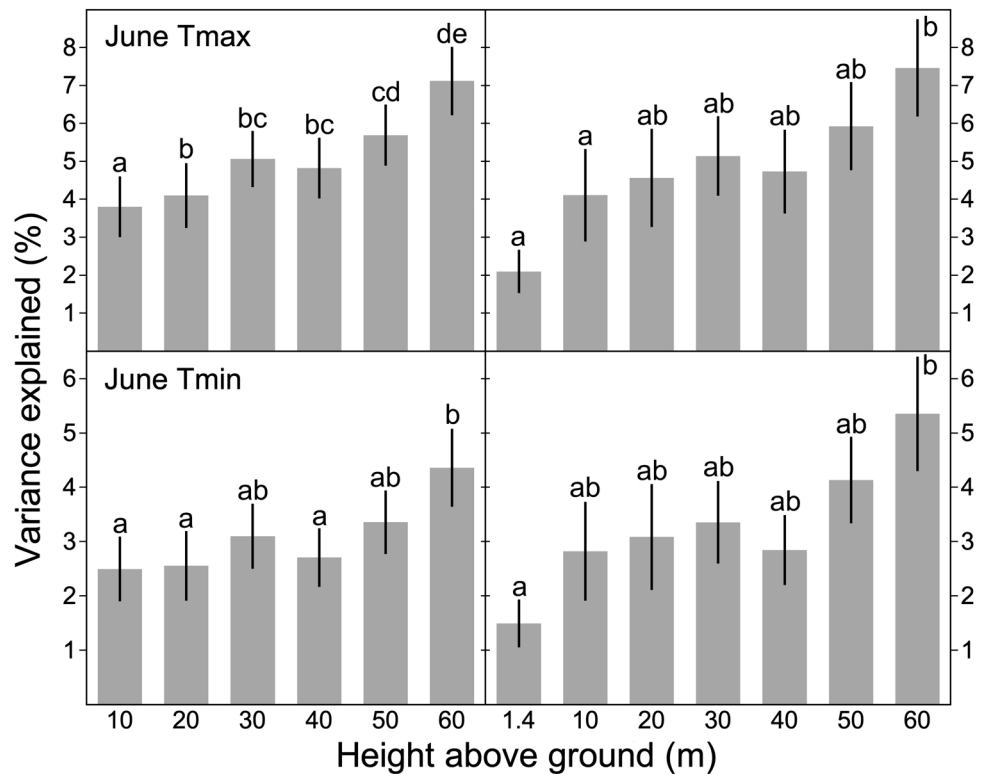


Table 4 Bootstrapped Pearson's correlation coefficients (r) between *Sequoiadendron* tree-ring chronologies and regional climatic variables

Height (m)	Correlation (r), 31 trees, 10–60 m				Correlation (r), 18 trees, 1.4–60 m			
	Jun	Jun	Apr	Sept	Jun	Jun	Apr	Sept
60	<i>-0.44*</i>	<i>-0.39*</i>	0.28	<i>0.33*</i>	<i>-0.42*</i>	<i>-0.38*</i>	0.23	<i>0.28</i>
50	<i>-0.40*</i>	<i>-0.34*</i>	0.27	<i>0.31*</i>	<i>-0.36*</i>	<i>-0.33*</i>	0.23	<i>0.28</i>
40	<i>-0.37*</i>	<i>-0.30*</i>	0.29	<i>0.33*</i>	<i>-0.33*</i>	<i>-0.28</i>	0.25	<i>0.28</i>
30	<i>-0.39*</i>	<i>-0.33*</i>	<i>0.39*</i>	<i>0.37*</i>	<i>-0.34*</i>	<i>-0.30</i>	0.28	<i>0.28</i>
20	<i>-0.33*</i>	<i>-0.27</i>	<i>0.39*</i>	<i>0.39*</i>	<i>-0.30</i>	<i>-0.26</i>	<i>0.35</i>	<i>0.34*</i>
10	-0.29	-0.22	<i>0.45*</i>	<i>0.41*</i>	<i>-0.26</i>	-0.22	<i>0.39*</i>	<i>0.36*</i>
1.4	na	na	na	na	-0.17	-0.14	0.27	<i>0.26</i>

Complementary analyses are for heights from 10–60 m (left, 31 trees) and 1.4–60 m (right, 18 trees). Climatic metrics are maximum (Tmax) and minimum (Tmin) temperature in June, snow water equivalent (SWE) for April 1, and standardized precipitation evapotranspiration index (SPEI) for the 12-month window ending in September. Window of analysis for SWE = 1940–2011 and 1902–2011 for Tmax, Tmin, and SPEI. Levels of significance indicated by italics for $P < 0.05$, bold for $P < 0.01$, * for $P < 0.001$

correlated with SPEI at $P < 0.001$, but lower trunk correlations were higher ($r = 0.42$ vs. 0.32).

Discussion

Updated and expanded *Sequoiadendron* ring-width chronologies

With trees of only 30 species documented > 1000 yr old (Liu et al. 2022), the addition or amendment of 9 location

chronologies spanning 928–1973 yr enhances the tree-ring catalog (St. George 2014). Constituent tree-level chronologies (17 > 1000 yr) derived from 61 *Sequoiadendron* show strong crossdating and a generally robust shared signal (Table S1, Fig. 1) that support a composite chronology (Fig. 2) similar to other assessments of this species (Brown et al. 1992; Hughes et al. 1996; Touchan et al. 2021). Of note is the addition of a nearly 2000-yr chronology at AC (Table 2), a grove not yet represented in dendrochronological study as it was recently acquired by the Save the Redwoods League for eventual transfer to Giant Sequoia

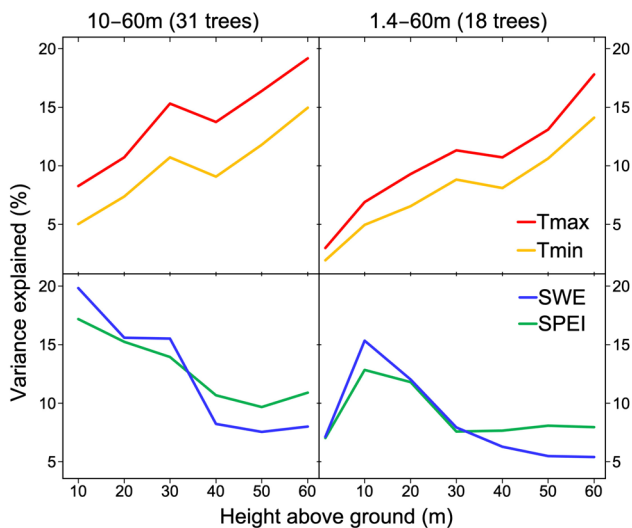


Fig. 5 Percent variance explained between *Sequoiadendron* tree-ring chronologies and regional climate variables by axial position (height above ground). Complementary analyses are for heights from 10–60 m (left, 31 trees) and 1.4–60 m (right, 18 trees). Tmax (maximum temperature) and Tmin (minimum temperature) are for June, SWE (snow water equivalent) is for April 1, and SPEI (standardized precipitation evapotranspiration index) is for the 12-month window ending in September. Window of analysis for SWE=1940–2011 and 1902–2011 for Tmax, Tmin, and SPEI

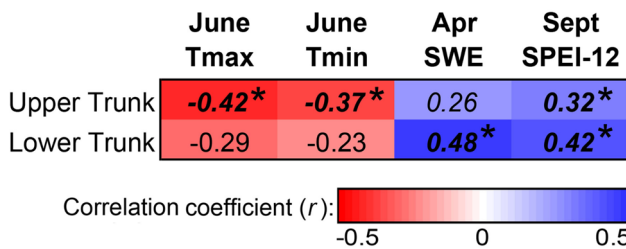


Fig. 6 Bootstrapped Pearson's correlation coefficients (r) for upper vs. lower trunk *Sequoiadendron* chronologies and regional climate variables. Upper and lower trunk chronologies are composed of 44 trees, most with 2 series per position. Tmax (maximum temperature) and Tmin (minimum temperature) are for June, SWE (snow water equivalent) is for April 1, and SPEI (standardized precipitation evapotranspiration index) is for the 12-month window ending in September. Correlations span the common window of 1940–2011 for SWE and 1902–2011 for the others. Red conveys strength for negative correlations and blue for positive correlations. Levels of significance indicated by italics for $P < 0.05$, bold for $P < 0.01$, * for $P < 0.001$

National Monument (Fimrite 2019). While ground-based *Sequoiadendron* dendrochronology is the norm, we include a component of within-trunk sampling of living trees at a level only achieved for a handful of tall conifer species (Sillett et al. 2021). The effort to attain and analyze samples spanned years, and these data are paired with intensive tree-level measurements and calculations (Sillett et al. 2015b,

2019b) providing an important compendium (Table S3). The within-tree sample design opens an array of research possibilities, and here we examine how climatic sensitivity varies with height above ground.

Axial variation of climate sensitivity and expression of low-growth years

Sequoiadendron augments the number of species with growth–climate relationships that vary with axial position on the main trunk (see Latte et al. 2016 Table 1 for partial list). Multiple approaches corroborate the general trends of increasing sensitivity to June Tmax and Tmin with height above ground and decreasing sensitivity to hydroclimate variables of SWE and SPEI with height above ground (except BH). Optimizing the relationship between tree ring and environmental metrics is a fundamental step in developing proxies that extend beyond historical records. Such analyses are often employed at the landscape level, targeting trees near range margins where climate is more limiting (Fritts 1976; Camarero et al. 2021). The same strategy can be used at the tree level, focusing on more sensitive positions along the trunk. Relatively weak dendroclimatic relationships at BH as well as PRI of low-growth years both indicate that irregular basal trunk morphology dampens climate-induced tree-ring signals. The buttressed region of large trunks in tall species such as *Eucalyptus regnans*, *Picea sitchensis*, *Pseudotsuga menziesii*, *Sequoia sempervirens*, and *Sequoiadendron giganteum* is so complex that 3D footprint analysis is necessary to extract functional diameters (e.g., $fDBH$) for allometric estimation of biomass and accurate carbon accounting (Dean et al. 2018; Kramer et al. 2018; Sillett et al. 2021). While basal sampling has clearly not hindered crossdating of *Sequoiadendron* (Douglass 1919), and such ring series have long supported successful climatic assessments (Hughes and Brown 1992; Touchan et al. 2021), dendroclimatic signals can be maximized by sampling above the buttress on large individuals such as used in this study (Table S1). Tree-climbing is a technical and time-intensive endeavor not available for all research, but these findings are applicable to fallen trunks that are well-preserved given *Sequoiadendron*'s extremely decay-resistant heartwood (Sillett et al. 2021). Remnant stumps are also present in some groves, and some may reach heights that reduce the influence of basal buttressing.

Contrasting axial relationships between *Sequoiadendron* radial growth and temperature versus hydroclimate variables may be influenced by temporal and spatial components of biophysical processes. June is a period of maximum light availability for photosynthesis combined with abundant soil water from snowmelt. Among 70 *Sequoiadendron* groves, snow cover persistence decreases from March to June followed by a ~3-month recession of soil moisture (Ray 2016).

During the early growing season, ring formation on *Sequoiadendron* is generally more apparent in upper than lower trunks (personal observations from variable coring dates) as assimilates are allocated from sources (foliage) to sinks (e.g., roots; Gower et al. 1995; Lacoïnte 2000). Hot temperatures in June greatly increase evaporative demand, and if air vapor pressure deficit drops too low, leaf stomata must close to maintain turgor and avoid embolism, thus limiting carbon assimilation during upper trunk ring formation (Zweifel et al. 2007; McDowell et al. 2008). *Sequoiadendron* exhibits strong stomatal regulation, especially in upper crown foliage, due to height-related increases in both light availability and water stress (Ambrose 2015, 2016, 2018; Williams et al. 2017, 2021). Patterns hold for both June T_{max} and T_{min}, possibly reflecting the spatial variation of source and sink limitations on ring formation during this time of year; high daytime temperature and evaporative demand limit carbon assimilation, and drier air at night limits the ability of trees to convert fixed carbon into biomass (Zweifel et al. 2021). Axial variation in sink limitations may explain the trend of increasing heartwood fungicide content (instead of ring formation) with height in closely related *S. sempervirens* (Sillett et al. 2022) and may also apply to *Sequoiadendron*.

As snowmelt dissipates, conifers of the Sierra Nevada become increasingly water stressed later in the growing season (Royce and Barbour 2001; Blankinship et al. 2014) when cell enlargement may be more active (and sensitive to environmental constraints) in the lower trunk, but more research on cambial phenology along the height gradient is needed to align phases of xylogenesis with seasonal timing (Monson et al. 2018). Decreasing water availability necessitates stronger stomatal control so trees can rehydrate growing tissues (Peters et al. 2023). Axial trends are generally stronger for SWE than SPEI which makes sense given that SPEI integrates temperature but does not adequately consider snowpack (Vicente-Serrano et al. 2010; Staudinger et al. 2014; Tian et al. 2021). In addition, drought-induced reductions in photosynthesis and water availability may cause a decrease in phloem conductivity that slows transport to the lower trunk (Salmon et al. 2019; Peters et al. 2020), causing increased sensitivity at lower heights as observed in several species (Bouriaud et al. 2005; Hoffmann et al. 2018). Moreover, structural complexity of old individual *Sequoiadendron*, which develop reiterated trunks, limbs up to 2 m diameter, crown spreads > 25 m, and crown depths > 70 m (Sillett et al. 2015b, 2019b), creates a dynamic environment for water availability, carbon assimilation, and environmental sensitivity (Niinemets 2007) that must influence axial relationships.

We document axial variation in dendroclimatic relationships for *Sequoiadendron* and propose several mechanisms, but some important considerations remain. Stored mobile carbon can act as a buffer for growth particularly during

stressful periods (Sala et al. 2012), and species-specific differences in non-structural carbohydrates mediated tree growth responses to a hot drought (2011–2012) in the southwestern US (Peltier et al. 2021). Lagged growth–climate dynamics may explain differential axial relationships for *P. contorta*, where hot and dry early summer limit upper trunk growth while prior year’s conditions drive lower trunk sensitivity (Chhin et al. 2010). We use regionally coherent inter-annual variation (Fig. 1) and climatic sensitivities (Fig. 3) as the basis for grouped analysis, but differences in landscape position may also influence axial relationships (van der Maaten-Theunissen and Bouriaud 2012). In the Sierra Nevada, snow cover persistence varies with topography, elevation, and aspect (Ray 2016), time to reach soil dryness ranges by up to 4 weeks due to heterogeneity (Bales et al. 2011), and *Sequoiadendron* canopy water content during drought varies with geological substrate and topography (Paz-Kagan et al. 2018). Further analysis would benefit from consideration of interactions of co-occurring stresses as well as finer-resolution climatic metrics. Our approach prioritizes a maximum climate window (e.g., 1900–present), which limits inclusion of some of the highest samples; so, although we far exceed the upper heights of comparable analyses, concentrating future sampling on near-treetop positions, including reiterated trunks, could further elucidate relationships and inform proposed mechanisms.

Conclusion

Within-trunk sampling of *Sequoiadendron* provides spatially explicit data permitting ring-width chronologies (at tree-, location-, and regional-levels) and documentation of axial variation in dendroclimatic sensitivities that can be leveraged to maximize environmental reconstructions for this long-lived species (> 3000 yr; RMTRR 2023). Basal positions of large trees have been targeted for fire histories and are easily accessible from ground, but their irregular morphology can mute climatic signals and expression of low-growth years compared to higher above the ground. While *Sequoiadendron* employs multiple strategies to maintain favorable water status during drought (Chin and Sillett 2016; Ambrose et al. 2016, 2018; Williams et al. 2021), hot June temperatures and low soil moisture curtail radial growth with axial trends likely attributable to seasonal timing of intra-trunk ring formation, stomatal regulation, and maintenance of stem turgor (Peters et al. 2023). Such relationships are relevant for understanding carbon dynamics and biophysical responses to changing conditions as the Sierra Nevada experiences hotter droughts (Griffin and Anchukaitis 2014; Diffenbaugh et al. 2015) and reduced snowpack (Ashfaq et al. 2013; Berg and Hall 2017). Axial variation in dendroclimatic relationships should be explored for other tall

conifers of western North America that have been similarly sampled (*P. sitchensis*, *P. menziesii*, *S. sempervirens*) and have divergent ecologies (Ambrose et al. 2009; Kramer et al. 2018; Chin and Sillett 2019; Sillett et al. 2021).

Supplementary Information The online version contains supplementary material available at <https://doi.org/10.1007/s00468-024-02517-6>.

Acknowledgements We thank the following for contributions to field work: A. Ambrose, M. Antoine, W. Baxter, W. Blozan, J. Campbell-Spickler, E. Coonen, T. Dawson, J. Freund, G. Koch, R. Kramer, R. Næsborg, G. Renzullo, K. Scarla, R. Van Pelt, and C. Williams. We thank Calaveras Big Trees State Park, Yosemite National Park, Sequoia and Kings Canyon National Parks, Mountain Home State Demonstration Forest, Sequoia National Monument University of California (Whitaker Forest), and Save the Redwoods League for access to these forests for this and prior research.

Authors contribution Study concept and design: AC, SS. Fieldwork team leader and data collection: SS. Crossdating and chronology building: AC. Radial increments and interpolations: SS. Dendroclimatic analysis: AC. Analysis of axial variation: AC, SS. First draft: AC. Manuscript writing and revision: AC, SS. Figures: AC, SS.

Funding This work was supported by Save the Redwoods League (Redwoods and Climate Change Initiative) and Kenneth L. Fisher (Chair in Redwood Forest Ecology at Cal Poly Humboldt).

Data availability Raw ring-width measurements for crossdated series are available in Supplementary Table S3.

Declarations

Conflict of interest The authors have no relevant financial or non-financial interests to disclose.

Open Access This article is licensed under a Creative Commons Attribution 4.0 International License, which permits use, sharing, adaptation, distribution and reproduction in any medium or format, as long as you give appropriate credit to the original author(s) and the source, provide a link to the Creative Commons licence, and indicate if changes were made. The images or other third party material in this article are included in the article's Creative Commons licence, unless indicated otherwise in a credit line to the material. If material is not included in the article's Creative Commons licence and your intended use is not permitted by statutory regulation or exceeds the permitted use, you will need to obtain permission directly from the copyright holder. To view a copy of this licence, visit <http://creativecommons.org/licenses/by/4.0/>.

References

- Ambrose AR, Sillett SC, Dawson TE (2009) Effects of tree height on branch hydraulics, leaf structure and gas exchange in California redwoods. *Plant Cell Environ* 32:743–757. <https://doi.org/10.1111/j.1365-3040.2009.01950.x>
- Ambrose AR, Baxter WL, Wong CS, Næsborg R, Williams CB, Dawson TE (2015) Contrasting drought-response strategies in California redwoods. *Tree Physiol* 35:453–469. <https://doi.org/10.1093/treephys/tpv016>
- Ambrose AR, Baxter WL, Wong CS, Burgess SSO, Williams CB, Næsborg R, Koch GW, Dawson TE (2016) Hydraulic constraints modify optimal photosynthetic profiles in giant sequoia trees. *Oecologia* 182:713–730. <https://doi.org/10.1007/s00442-016-3705-3>
- Ambrose AR, Baxter WL, Martin RE, Francis E, Asner GP, Nydick KR, Dawson TE (2018) Leaf- and crown-level adjustments help giant sequoias maintain favorable water status during severe drought. *For Ecol Manag* 419–420:257–267. <https://doi.org/10.1016/j.foreco.2018.01.012>
- Ashfaq M, Ghosh S, Kao SC, Bowling LC, Mote P, Touma D, Rauscher SA, Diffenbaugh NS (2013) Near-term acceleration of hydroclimatic change in the western U.S. *J Geophys Res Atmos* 118:10676–10693. <https://doi.org/10.1002/jgrd.50816>
- Bales RC, Hopmans JW, O'Geen AT, Meadows M, Hartsough PC, Kirchner P, Hunsaker CT, Beaudette D (2011) Soil moisture response to snowmelt and rainfall in a Sierra Nevada mixed-conifer forest. *Vadose Zone J* 10:786–799. <https://doi.org/10.2136/vzj2011.0001>
- Begum S, Nakaba S, Yamagishi Y, Oribe Y, Funada R (2013) Regulation of cambial activity in relation to environmental conditions: Understanding the role of temperature in wood formation of trees. *Physiol Plant* 147:46–54. <https://doi.org/10.1111/j.1399-3054.2012.01663.x>
- Benjamini Y, Hochberg Y (1995) Controlling the false discovery rate: A practical and powerful approach to multiple testing. *J R Stat Soc Ser B (methodol)* 57:289–300. <https://doi.org/10.1111/j.2517-6161.1995.tb02031.x>
- Berg N, Hall A (2017) Anthropogenic warming impacts on California snowpack during drought. *Geophys Res Lett* 44:2511–2518. <https://doi.org/10.1002/2016GL072104>
- Blankinship JC, Meadows MW, Lucas RG, Hart SC (2014) Snowmelt timing alters shallow but not deep soil moisture in the Sierra Nevada. *Water Resour Res* 50:1448–1456. <https://doi.org/10.1002/2013WR014541>
- Bouriaud O, Leban JM, Bert D, Deleuze C (2005) Intra-annual variations in climate influence growth and wood density of Norway spruce. *Tree Physiol* 25:651–660. <https://doi.org/10.1093/treephys/25.6.651>
- Brookhouse M, Brack C (2008) The effect of age and sample position on eucalypt tree-ring width series. *Can J for Res* 38:1144–1158. <https://doi.org/10.1139/X07-184>
- Brown PM, Hughes MK, Baisan CH, Swetnam TW, Caprio AC (1992) Giant sequoia ring-width chronologies from the central Sierra Nevada, California. *Tree-Ring Bull* 52:1–14
- Bunn AG (2008) A dendrochronology program library in R (dplR). *Dendrochronologia* 26:115–124. <https://doi.org/10.1016/j.dendro.2008.01.002>
- Buttò V, Deslauriers A, Rossi S, Rozenberg P, Shishov V, Morin H (2020) The role of plant hormones in tree-ring formation. *Trees* 34:315–335. <https://doi.org/10.1007/s00468-019-01940-4>
- Cabon A, Kannenberg SA, Arain A, Babst F, Baldocchi D et al (2022) Cross-biome synthesis of source versus sink limits to tree growth. *Science* 376:758–761
- Camarero JJ, Gazol A, Sangüesa-Barreda G, Vergarechea M, Alfaro-Sánchez R, Cattaneo N, Vicente-Serrano SM (2021) Tree growth is more limited by drought in rear-edge forests most of the times. *For Ecosyst*. <https://doi.org/10.1186/s40663-021-00303-1>
- Carroll AL, Sillett SC (2023) Overcoming crossdating challenges to generate ring-width chronologies for *Sequoia sempervirens* across its native range. *Dendrochronologia*. <https://doi.org/10.1016/j.dendro.2023.126063>
- Carroll AL, Sillett SC, Kramer RD (2014) Millennium-scale crossdating and interannual climate sensitivities of standing California redwoods. *PLoS ONE*. <https://doi.org/10.1371/journal.pone.0102545>
- Chhin S, Hogg EH, Lieffers VJ, Huang S (2010) Growth–climate relationships vary with height along the stem in lodgepole pine. *Tree Physiol* 30:335–345. <https://doi.org/10.1093/treephys/tpq120>

- Chin ARO, Sillett SC (2016) Phenotypic plasticity of leaves enhances water-stress tolerance and promotes hydraulic conductivity in a tall conifer. *Am J Bot* 103:796–807. <https://doi.org/10.3732/ajb.1600110>
- Chin ARO, Sillett SC (2019) Within-crown plasticity in leaf traits among the tallest conifers. *Am J Bot* 106:1–13. <https://doi.org/10.1002/ajb2.1230>
- Cook ER, Kairiukstis L (1990) *Methods of dendrochronology*. Kluwer, Dordrecht
- Cook ER, Seager R, Cane MA, Stahle DW (2007) North American drought: reconstructions, causes, and consequences. *Earth Sci Rev* 81:93–134
- Cook ER (1985) *A time series analysis approach to tree-ring standardization*. Dissertation, University of Arizona, Tucson
- De Micco V, Carrer M, Rathgeber CB, Julio Camarero J, Voltas J, Cherubini P, Battipaglia G (2019) From xylogenesis to tree rings: wood traits to investigate tree response to environmental changes. *IAWA J* 40:155–182
- Dean C, Kirkpatrick JB, Osborn J, Doyle RB, Fitzgerald NB, Roxburgh SH (2018) Novel 3D geometry and models of the lower regions of large trees for use in carbon accounting of primary forests. *AoB Plants* 10:1–20. <https://doi.org/10.1093/aobpla/ply015>
- Diffenbaugh NS, Swain DL, Touma D, Lubchenco J (2015) Anthropogenic warming has increased drought risk in California. *Proc Natl Acad Sci USA* 112:3931–3936. <https://doi.org/10.1073/pnas.1422385112>
- Douglas AE (1919) *Climate cycles and tree-growth: a study of the annual rings of trees in relation to climate and solar activity*, vol I. Carnegie Institute of Washington, Pub Num 289, Washington, D.C.
- Eisinga R, Heskes T, Pelzer B, Te Grotenhuis M (2017) Exact p-values for pairwise comparison of Friedman rank sums, with application to comparing classifiers. *BMC Bioinforma*. <https://doi.org/10.1186/s12859-017-1486-2>
- Fimrite, P (2019) Biggest private sequoia grove to be preserved in deal with Redwoods League. *San Francisco Chronicle*. 17 September 2019
- Fritts HC (1976) *Tree rings and climate*. Academic Press, London
- Gazol A, Camarero JJ, Sangüesa-Barreda G, Sangüesa-Barreda G, Serra-Maluquer X, Sánchez-Salguero R, Coll L, Casals P (2020) Tree species are differently impacted by cumulative drought stress and present higher growth synchrony in dry places. *Front for Glob Change*. <https://doi.org/10.3389/ffgc.2020.573346>
- Gower ST, Isebrands JG, Sheriff DW (1995) Carbon allocation and accumulation in conifers. In: Smith WK, Hinckley TM (eds) *Resource physiology of conifers*. Academic Press, San Diego, pp 217–254
- Griffin D, Anchukaitis KJ (2014) How unusual is the 2012–2014 California drought? *Geophys Res Lett* 41:9017–9023. <https://doi.org/10.1002/2014GL062433>
- Hoffmann N, Schall P, Ammer C, Leder B, Vor T (2018) Drought sensitivity and stem growth variation of nine alien and native tree species on a productive forest site in Germany. *Agric Meteor* 256–257:431–444. <https://doi.org/10.1016/j.agrformet.2018.03.008>
- Holmes RL (1983) Computer-assisted quality control in tree-ring dating and measurement. *Tree-Ring Bull* 43:69–75
- Hughes MK, Brown PM (1992) Drought frequency in central California since 101 B.C. recorded in giant sequoia tree rings. *Clim Dyn* 6:161–167
- Hughes MK, Touchan R, Brown PM (1996) A multimillennial network of giant sequoia chronologies for dendroclimatology. In: Dean JS, Meko DM, Swetnam TW (eds) *Tree rings, environment, and humanity: Proceedings of the international conference*, Tucson, Arizona, 17–21 May 1994. *Radiocarbon*, Tucson, pp 225–234
- Huning LS, AghaKouchak A (2020) Approaching 80 years of snow water equivalent information by merging different data streams. *Sci Data* 7:333. <https://doi.org/10.1038/s41597-020-00649-1>
- Ishii HR, Sillett SC, Carroll AL (2017) Crown dynamics and wood production of Douglas-fir trees in an old-growth forest. *For Ecol Manag* 384:157–168. <https://doi.org/10.1016/j.foreco.2016.10.047>
- Kerhoulas LP, Kane JM (2012) Sensitivity of ring growth and carbon allocation to climatic variation vary within ponderosa pine trees. *Tree Physiol* 32:14–23. <https://doi.org/10.1093/treephys/tpr112>
- Koch GW, Sillett SC, Jennings GM, Davis SD (2004) The limits to tree height. *Nature* 428:851–854. <https://doi.org/10.1038/nature02417>
- Körner C (2015) Paradigm shift in plant growth control. *Opinion in Plant Biol* 25:107–114. <https://doi.org/10.1016/j.pbi.2015.05.003>
- Kramer RD, Sillett SC, Van Pelt R (2018) Quantifying aboveground components of *Picea sitchensis* for allometric comparisons among tall conifers in North American rainforests. *For Ecol Manag* 430:59–77. <https://doi.org/10.1016/j.foreco.2018.07.039>
- Lacointe A (2000) Carbon allocation among tree organs: A review of basic processes and representation in functional-structural tree models. *Ann for Sci* 57:521–533. <https://doi.org/10.1051/forest:2000139>
- Latte N, Lebourgeois F, Claessens H (2016) Growth partitioning within beech trees (*Fagus sylvatica* L.) varies in response to summer heat waves and related droughts. *Trees* 30:189–201. <https://doi.org/10.1007/s00468-015-1288-y>
- Liu J, Xia S, Zeng D, Liu C, Li Y, Yang W, Yang B, Zhang J, Slik F, Lindenmayer DB (2022) Age and spatial distribution of the world's oldest trees. *Conserv Biol*. <https://doi.org/10.1111/cobi.13907>
- Lorimer CG, Dahir SE, Singer MT (1999) Frequency of partial and missing rings in *Acer saccharum* in relation to canopy position and growth rate. *Plant Ecol* 143:189–202
- McDowell N, Pockman WT, Allen CD, Breshears DD, Cobb N, Kolb T, Plaut J, Sperry J, West A, Williams DG, Ypez EA (2008) Mechanisms of plant survival and mortality during drought: why do some plants survive while others succumb to drought? *New Phytol* 178:719–739
- Monson RK, Szejner P, Belmecheri S, Morino KA, Wright WE (2018) Finding the seasons in tree ring stable isotope ratios. *Am J Bot* 105:819–821. <https://doi.org/10.1002/ajb2.1083>
- Niinemets Ü (2007) Photosynthesis and resource distribution through plant canopies. *Plant Cell Environ* 30:1052–1071. <https://doi.org/10.1111/j.1365-3040.2007.01683.x>
- Nydic KR, Stephenson NL, Ambrose AR, Asner GP, Baxter WL, Das AJ, Dawson TE, Martin RE, Paz-Kagan T (2018) Leaf to landscape responses of giant sequoia to hotter drought: an introduction and synthesis for the special section. *For Ecol Manag* 419–420:249–256. <https://doi.org/10.1016/j.foreco.2018.03.028>
- Paz-Kagan T, Vaughn NR, Martin RE, Brodrick P, Stephenson NL, Das AJ, Nydic KR, Asner GP (2018) Landscape-scale variation in canopy water content of giant sequoias during drought. *For Ecol Manag* 419–420:291–304. <https://doi.org/10.1016/j.foreco.2017.11.018>
- Peltier DM, Guo J, Nguyen P, Bangs M, Wilson M et al (2021) Temperature memory and non-structural carbohydrates mediate legacies of a hot drought in trees across the southwestern USA. *Tree Physiol* 42:71–85. <https://doi.org/10.1093/treephys/tpab091>
- Peters RL, von Arx G, Nievergelt D, Ibrom A, Stillhard J, Trotsiuk V, Mazurkiewicz A, Babst F (2020) Axial changes in wood functional traits have limited net effects on stem biomass increment in European beech (*Fagus sylvatica*). *Tree Physiol* 40:498–510. <https://doi.org/10.1093/treephys/tpaa002>
- Peters RL, Stepe K, Pappas C, Zweifel R, Babst F, Dietrich L, von Arx G, Poyatos R, Fonti M, Fonti P, Grossiord C, Gharum M, Buchmann N, Steger DN, Kahmen A (2023) Daytime stomatal

- regulation in mature temperate trees prioritizes stem rehydration at night. *New Phytol* 239:533–546. <https://doi.org/10.1111/nph.18964>
- Pierce DW, Kalansky JF, Cayan DR (2018) Climate, drought, and sea level rise scenarios for the Fourth California Climate Assessment. California's Fourth Climate Change Assessment, California Energy Commission. Pub Num CNRACEC-2018–006
- Pohlert T (2022) PMCMRplus: Calculate pairwise multiple comparisons of mean rank sums extended. R package version 1.9.6. <https://CRAN.R-project.org/package=PMCMRplus>
- R Core Team (2023) R: A language and environment for statistical computing. R Foundation for Statistical Computing, Vienna, Austria. <https://www.R-project.org/>
- Rathgeber CBK, Cuny HE, Fonti P (2016) Biological basis of tree-ring formation: a crash course. *Front Plant Sci* 7:734. <https://doi.org/10.3389/fpls.2016.00734>
- Ray R (2016) Moisture stress indicators in giant sequoia groves in the southern Sierra Nevada of California. *Vadose Zone J* 15, USA. <https://doi.org/10.2136/vzj2016.03.0018>
- RMTRR, Rocky Mountain Tree-Ring Research (2023) OLDLIST, A database of old trees. <http://www.rmtrr.org/oldlist.htm>
- Royce EB, Barbour MG (2001) Mediterranean climate effects. I. Conifer water use across a sierra nevada ecotone. *Am J Bot* 88:911–918. <https://doi.org/10.2307/2657044>
- Sala A, Woodruff DR, Meinzer FC (2012) Carbon dynamics in trees: feast or famine? *Tree Physiol* 32:764–775. <https://doi.org/10.1093/treephys/tp143>
- Salmon Y, Dietrich L, Sevanto S, Hölttä T, Dannoura M, Epron D (2019) Drought impacts on tree phloem: from cell-level responses to ecological significance. *Tree Physiol* 39:173–191. <https://doi.org/10.1093/treephys/tpy153>
- Sillett SC, Van Pelt R, Kramer RD, Carroll AL, Koch GW (2015a) Biomass and growth potential of *Eucalyptus regnans* up to 100 m tall. *For Ecol Manag* 348:78–91. <https://doi.org/10.1016/j.foreco.2015.03.046>
- Sillett SC, Van Pelt R, Carroll AL, Kramer RD, Ambrose AR, Trask D (2015b) How do tree structure and old age affect growth potential of California redwoods? *Ecol Monogr* 85:181–212. <https://doi.org/10.1890/14-1016.1>
- Sillett SC, Van Pelt R, Carroll AL, Campbell-Spickler J, Coonen EJ, Iberle B (2019a) Allometric equations for *Sequoia sempervirens* in forests of different ages. *For Ecol Manag* 433:349–363. <https://doi.org/10.1016/j.foreco.2018.11.016>
- Sillett SC, Van Pelt R, Carroll AL, Campbell-Spickler J, Antoine ME (2019b) Structure and dynamics of forests dominated by *Sequoiadendron giganteum*. *For Ecol Manag* 448:218–239. <https://doi.org/10.1016/j.foreco.2019.05.064>
- Sillett SC, Van Pelt R, Carroll AL, Campbell-Spickler J, Antoine ME (2020) Aboveground biomass dynamics and growth efficiency of *Sequoia sempervirens* forests. *For Ecol Manag*. <https://doi.org/10.1016/j.foreco.2019.117740>
- Sillett SC, Kramer RD, Van Pelt R, Carroll AL, Campbell-Spickler J, Antoine ME (2021) Comparative development of the four tallest conifer species. *For Ecol Manag*. <https://doi.org/10.1016/j.foreco.2020.118688>
- Sillett SC, Antoine ME, Carroll AL, Graham ME, Chin ARO, Van Pelt R (2022) Rangeland climatic sensitivities and non-timber values of tall *Sequoia sempervirens* forests. *For Ecol Manag*. <https://doi.org/10.1016/j.foreco.2022.120573>
- Speer JH (2010) Fundamentals of tree-ring research. The University of Arizona Press, Tucson
- St. George S, (2014) An overview of tree-ring width records across the Northern Hemisphere. *Quat Sci Rev* 95:132–150. <https://doi.org/10.1016/j.quascirev.2014.04.029>
- Staudinger M, Stahl K, Seibert J (2014) A drought index accounting for snow. *Water Resour Res* 50:7861–7872. <https://doi.org/10.1002/2013WR015143>
- Stephenson NL, Das AJ, Ampersee NJ, Cahill KG, Caprio AC, Sanders JE, Williams AP (2018) Patterns and correlates of giant sequoia foliage dieback during California's 2012–2016 hotter drought. *For Ecol Manag* 419–420:268–278. <https://doi.org/10.1016/j.foreco.2017.10.053>
- Swetnam TW, Baisan CH, Caprio AC, Brown PM, Touchan R, Anderson RS, Hallett DJ (2009) Multi-millennial fire history of the giant forest, Sequoia National Park, California, USA. *Fire Ecol* 5:120–150. <https://doi.org/10.4996/fireecology.0503120>
- Tian L, Zhang B, Wu P (2021) A global dataset of standardized moisture anomaly index incorporating snow dynamics from 1948 to 2010. *Earth System Sci Data* 14:2259–2278. <https://doi.org/10.5194/essd-2021-399>
- Touchan R, Black B, Shamir E, Hughes MK, Meko DM (2021) A multimillennial snow water equivalent reconstruction from giant sequoia tree rings. *Clim Dyn* 56:1507–1518. <https://doi.org/10.1007/s00382-020-05548-0>
- Vaganov EA, Anchukaitis KJ, Evans MN (2011) How well understood are the processes that create dendroclimatic records? A mechanistic model of the climatic control on conifer tree-ring growth dynamics. In: Hughes MK, Swetnam TW, Diaz HF (eds) *Dendroclimatology: progress and prospects*. Springer, Dordrecht, pp 37–75
- van der Maaten-Theunissen M, Bouriaud O (2012) Climate–growth relationships at different stem heights in silver fir and Norway spruce. *Can J for Res* 42:958–969. <https://doi.org/10.1139/x2012-046>
- Vicente-Serrano SM, Beguería S, López-Moreno JI (2010) A multi-scalar drought index sensitive to global warming: the standardized precipitation evapotranspiration index. *J Clim* 23:1696–1718. <https://doi.org/10.1175/2009JCLI2909.1>
- Wang T, Hamann A, Spittlehouse DL, Murdock TQ (2012) Climate-WNA—high-resolution spatial climate data for western North America. *J Appl Meteorol Climatol* 51:16–29. <https://doi.org/10.1175/JAMC-D-11-043.1>
- Wigley TML, Briffa KR, Jones PD (1984) On the average value of correlated time series, with applications in dendroclimatology and hydrometeorology. *J Clim Appl Meteor* 23:201–213
- Williams CB, Næsberg R, Dawson TE (2017) Coping with gravity: the foliar water relations of giant sequoia. *Tree Physiol* 37:1312–1326. <https://doi.org/10.1093/treephys/tpx074>
- Williams CB, Reese Næsberg R, Ambrose AR, Baxter WL, Koch GW, Dawson TE (2021) The dynamics of stem water storage in the tops of earth's largest trees - *Sequoiadendron giganteum*. *Tree Physiol* 41:2262–2278. <https://doi.org/10.1093/treephys/tpab078>
- Woodruff DR, Bond BJ, Meinzer FC (2004) Does turgor limit growth in tall trees? *Plant Cell Environ* 27:229–236. <https://doi.org/10.1111/j.1365-3040.2003.01141.x>
- Zang C, Biondi F (2015) Treeclim: an R package for the numerical calibration of proxy climate relationships. *Ecography* 38:431–436. <https://doi.org/10.1111/ecog.01335>
- Zhang T, Huang L, Zhang R, Gao Y, Hu D, Yu S, Jiang S (2020) The impacts of climatic factors on radial growth patterns at different stem heights in Schrenk spruce (*Picea schrenkiana*). *Trees* 34:163–175. <https://doi.org/10.1007/s00468-019-01908-4>
- Zweifel R, Steppe K, Sterck FJ (2007) Stomatal regulation by microclimate and tree water relations: interpreting ecophysiological field data with a hydraulic plant model. *J Exp Bot* 58:2113–2131. <https://doi.org/10.1093/jxb/erm050>
- Zweifel R, Sterck F, Braun S et al (2021) Why trees grow at night. *New Phytol* 231:2174–2185. <https://doi.org/10.1111/nph.17552>

Publisher's Note Springer Nature remains neutral with regard to jurisdictional claims in published maps and institutional affiliations.